tvst

https://doi.org/10.1167/tvst.8.6.46

Article

Functional Relevance and Structural Correlates of Near Infrared and Short Wavelength Fundus Autofluorescence Imaging in *ABCA4*-Related Retinopathy

Philipp L. Müller[1–3], Johannes Birtel[1,2], Philipp Herrmann[1,2], Frank G. Holz[1,2], Peter Charbel Issa[4,5], and Martin Gliem[1,2,4,5]

[1] University of Bonn, Department of Ophthalmology, Bonn, Germany
[2] University of Bonn, Center for Rare Diseases Bonn (ZSEB), Bonn, Germany
[3] Moorfields Eye Hospital NHS Foundation Trust, London, UK
[4] Oxford Eye Hospital, Oxford University Hospitals NHS Foundation Trust, Oxford, UK
[5] University of Oxford, Nuffield Laboratory of Ophthalmology, Department of Clinical Neurosciences, Oxford, UK

Correspondence: Philipp Herrmann, Department of Ophthalmology, University of Bonn, Ernst-Abbe-Straße 2, D-53127 Bonn, Germany. e-mail: philipp.herrmann@ukbonn.de

Received: 12 June 2019
Accepted: 18 October 2019
Published: 20 December 2019

Keywords: Stargardt disease; retina; optical coherence tomography; microperimetry; structure–function correlation

Citation: Müller PL, Birtel J, Herrmann P, Holz FG, Charbel Issa P, Gliem M. Functional relevance and structural correlates of near infrared and short wavelength fundus autofluorescence imaging in *ABCA4*-related retinopathy. Trans Vis Sci Tech. 2019;8(6):46, https://doi.org/10.1167/tvst.8.6.46

Purpose: To evaluate the functional relevance and structural correlates of autofluorescence (AF) alterations under short-wavelength (SW) and near-infrared (NIR) excitation light in *ABCA4*-related retinopathy.

Methods: In this prospective, cross-sectional case series, 88 eyes of 44 patients with *ABCA4*-related retinopathy (mean age, 37.6 years; range, 9–77 years) underwent SW-AF and NIR-AF imaging. The AF images were graded for disease characteristic patterns by two independent readers and correlated with alterations in optical coherence tomography (OCT) and impairment of retinal sensitivity along a foveo-papillary line assessed by fundus-controlled microperimetry.

Results: A centrifugal sequence of AF patterns from atrophic lesions to homogeneous background was found for both AF modalities. The eccentricity of each AF pattern in NIR-AF was larger compared to those in SW-AF ($P < 0.001$). Increasing eccentricity of each pattern correlated with increasing retinal sensitivity. The distant border of the zone of hyperfluorescent flecks in SW-AF and hypoautofluorescent flecks in NIR-AF correlated with the margins of the ellipsoid zone loss in OCT ($r = 0.979$ and $r = 0.971$, $P < 0.001$). The expansion of hypofluorescent flecks in SW-AF was associated with the boundaries of external limiting membrane loss ($r = 0.933$, $P < 0.001$).

Conclusions: SW-AF and NIR-AF revealed a characteristic sequence of AF patterns that correlated with functional and structural alterations, suggesting different stages in disease progression.

Translational Relevance: Alterations in NIR-AF exceeded those in SW-AF images, substantiating the hypothesis of different AF origins and suggesting NIR-AF as surrogate marker for early disease-related changes.

Introduction

ABCA4-related retinopathy (Online Mendelian Inheritance in Man, no. 601691) is one of the most frequent causes for inherited retinal degeneration and vision loss in early life.[1–3] It is caused by autosomal-recessive mutations in the *ATP-binding cassette subfamily A member 4* gene (*ABCA4*).[4,5] Dysfunction or loss of function of ABCA4 leads to excessive accumulation of lipofuscin in the retinal pigment epithelium (RPE), leading to retinal atrophy and associated loss of vision.[5,6] Based on the improved understanding of underlying disease mechanisms, several treatment options are currently being developed.[7] However, there is still uncertainty about suitable outcome measures for the sensitive detection of potential treatment effects. Such measures should ideally be easy to acquire, have high test-retest reliability, should reflect functional impairment of

the patients, and be predictive for long-term progression based on short-term changes.

Patients with *ABCA4*-related retinopathy show characteristic findings on fundus autofluorescence (AF) imaging using short-wavelength excitation light (SW-AF), including a generally increased AF intensity and distinct flecked patterns of increased and/or decreased AF.[8–12] An alternative AF imaging modality is near-infrared autofluorescence (NIR-AF) imaging, which is assumed to derive mainly from melanin and melano-lipofuscin within RPE cells and choroidal melanocytes.[13,14] It has been shown that NIR-AF images display characteristic differences in *ABCA4*-related retinopathy compared to SW-AF: NIR-AF patterns are more likely hypoautofluorescent, the extent of hypofluorescent lesions exceed those in SW-AF, and alterations seem to precede those in SW-AF.[15–20] In individual studies, both AF modalities have been correlated with changes on optical coherence tomography (OCT)[16–18,21,22] and functional measures.[12,20,23,24]

It has been proposed that different disease stages in *ABCA4*-related retinopathy can be investigated in detail along a foveo-papillary line.[14] However, a systematic qualitative and quantitative evaluation of individual AF patterns in SW-AF and NIR-AF as criteria for different disease stages has not yet performed in a larger cohort.

For this reason, the distribution of different AF patterns on SW-AF and NIR-AF images along a foveo-papillary line was investigated and correlated with OCT and fundus-controlled microperimetry data in a large cohort of patients with *ABCA4*-related retinopathy. Knowledge of different AF patterns and their functional and structural correlates as a susceptible marker for different disease stages may not only be of relevance for a better understanding of underlying disease mechanisms but also for a more sensitive detection of treatment effects in upcoming interventional trials.

Methods

This prospective, monocenter, cross-sectional case series was performed at the Department of Ophthalmology of the University of Bonn, Germany. The study was in adherence with the tenets of the declaration of Helsinki. Institutional review board approval (Ethikkommission, Medizinischen Fakultät, Rheinische Friedrich-Wilhelms-Universität Bonn, Germany) and patients' informed consent were obtained.

Patients with *ABCA4*-related retinopathy were recruited from a clinic for rare retinal diseases. Inclusion criteria comprised the presence of at least one disease-causing mutation in *ABCA4* and a phenotype consistent with *ABCA4*-related retinopathy, including RPE atrophy and flecks.[25] Insufficient pupil dilation, additional retinal pathology, previous vitreoretinal surgery, or other ocular comorbidities substantially affecting visual function (e.g., significant media opacity, amblyopia, or optic nerve disease) led to exclusion.

Image Acquisition

All patients underwent a comprehensive ophthalmologic examination including best corrected visual acuity (BCVA) testing using Early Treatment Diabetic Retinopathy Study charts, slit lamp examination, indirect ophthalmoscopy, full-field ERG (Toennies Multiliner Vision 1.70; Toennies, Höchberg, Germany) testing, and a dedicated imaging protocol. The imaging protocol consisted of fundus photography (Visucam; Carl Zeiss Meditec, Jena, Germany), SW-AF (488 nm) and NIR-AF (787 nm) imaging using confocal scanning laser ophthalmoscopy (cSLO) (Spectralis HRA; Heidelberg Engineering, Heidelberg, Germany), spectral-domain OCT (880 nm) (Spectralis HRA+OCT; Heidelberg Engineering), and mesopic fundus-controlled perimetry using confocal microperimetry (Macular Integrity Assessment [MAIA]; CenterVue, Padova, Italy).

For AF images, the field of view was set to 55° and 30° (centered on the fovea). Within the manufacturer's software, high-resolution mode (1536 × 1536 pixels) with and without normalization was utilized, and a minimum of 50 frames per image was automatically aligned and averaged to optimize the signal-to-noise ratio. SD-OCT was performed with single horizontal and vertical line scans centered on the fovea as well as volume scans (25° × 30°, 61 scans) with at least 20 frames per scan averaged. Fundus-controlled perimetry was performed using the MAIA device, which has an inbuilt cSLO (830 nm, 36.5° × 36.5°, 25 frames per second) that enables automated real-time fundus tracking. The protocol was comparable, as described previously.[26] Briefly, after 20 minutes of adaptation to the red test background luminance at 1.27 cd/m^2, retinal sensitivity was obtained using achromatic (400–800 nm) Goldmann III stimuli of 200-millisecond duration and a 4-2 staircase strategy of luminance comprising an dynamic range of 3.6 log units (0.08–318.5 cd/m^2).[27] The resulting point-wise retinal sensitivity can be exported either as values (36–0 dB) or as a cSLO image with

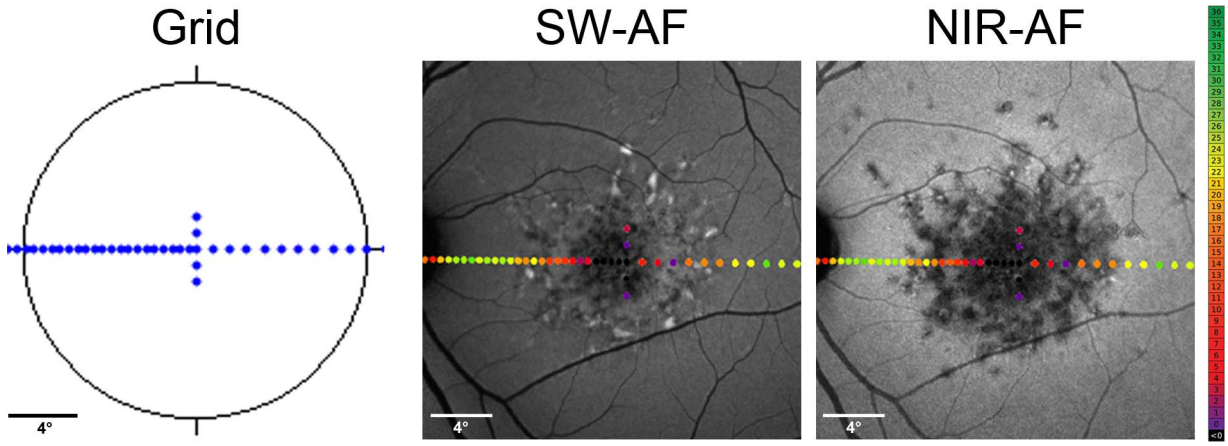

Figure 1. Microperimetry and image analysis. Using fundus-controlled perimetry, retinal sensitivity was examined at 50 loci along a horizontal line through the foveal center covering 30° of the central visual field with dense testing points between fovea and optic nerve head (*left*). For structure–function correlation, perimetric results were aligned and overlaid with SW-AF (*middle*) and NIR-AF images (*right*).

color-coded dots at the respective retinal locations (gradually, green for normal retinal sensitivity, yellow for moderate functional impairment, red for severe functional impairment, and black for no perception). To reduce learning effects, one full perimetric test was performed in each eye before the examination was executed. The custom-made test pattern was adapted from the foveo-papillary profile developed by Cideciyan et al.[23] (Fig. 1).

Image Processing

The 30° nonnormalized SW-AF and NIR-AF images, as well as OCT-associated images, were exported from image management software (Heidelberg Eye Explorer, version 1.9.10.0; Heidelberg Engineering) and aligned with the fundus-controlled perimetry results (cSLO image with color-coded dots and sensitivity values) of the respective subject using at least five landmarks and a dedicated custom-written software (Multi-Modal Mapper).[28] The outcome was then overlaid using image-editing software (Photoshop CS 6.0; Adobe, San Jose, CA; Fig. 1).

Based on previously published data and the clinical experience with AF images in *ABCA4*-related retinopathy of different medical retina specialists (PLM, FGH, PCI, and MG),[15–20,29] six different AF patterns were defined as follows (Fig. 2, first row):

1. Atrophic lesions (AL) defined as circumscribed definitely decreased AF (≥90% darkness of the optic disc)[29];
2. Continuous dark pattern not fulfilling the criteria of definitely decreased AF (P4) defined as questionably decreased AF (50%–90% darkness of the optic disc)[29];
3. Flecked pattern dominated by flecks of decreased AF defined as (P3);
4. Flecked pattern dominated by flecks of increased AF defined as (P2);
5. Granular pattern not fitting in any of the other categories defined as (P1);
6. Homogeneous background defined as no pattern (NP).

The delineation of each AF pattern was performed in Photoshop CS 6.0 using the pencil tool (red lines in Fig. 2). The expansion of each individual pattern in SW and NIR-AF images from the fovea to the optic disc was measured using the integrated measurement tool of Photoshop CS 6.0 and the individual scaling factor provided by the Heidelberg Eye Explorer. If one pattern was not clearly delineable, the expansion of the respective AF pattern was set to 0. The retinal sensitivity within each AF pattern was compiled for each eye by taking the mean of all stimuli located (>50% of the stimulus size) inside the respective pattern. The expansion of the RPE loss, ellipsoid zone (EZ) loss, and external limiting membrane (ELM) loss in OCT images was delineated using the Heidelberg Eye Explorer, annotated on the associated infrared image, and then processed according to the AF images. The delineations and measurements were manually performed by two independent experienced readers (PLM and JB) masked to the results of each other. For further analysis, the mean of both readers was used.

For subgroup analysis, patients were further

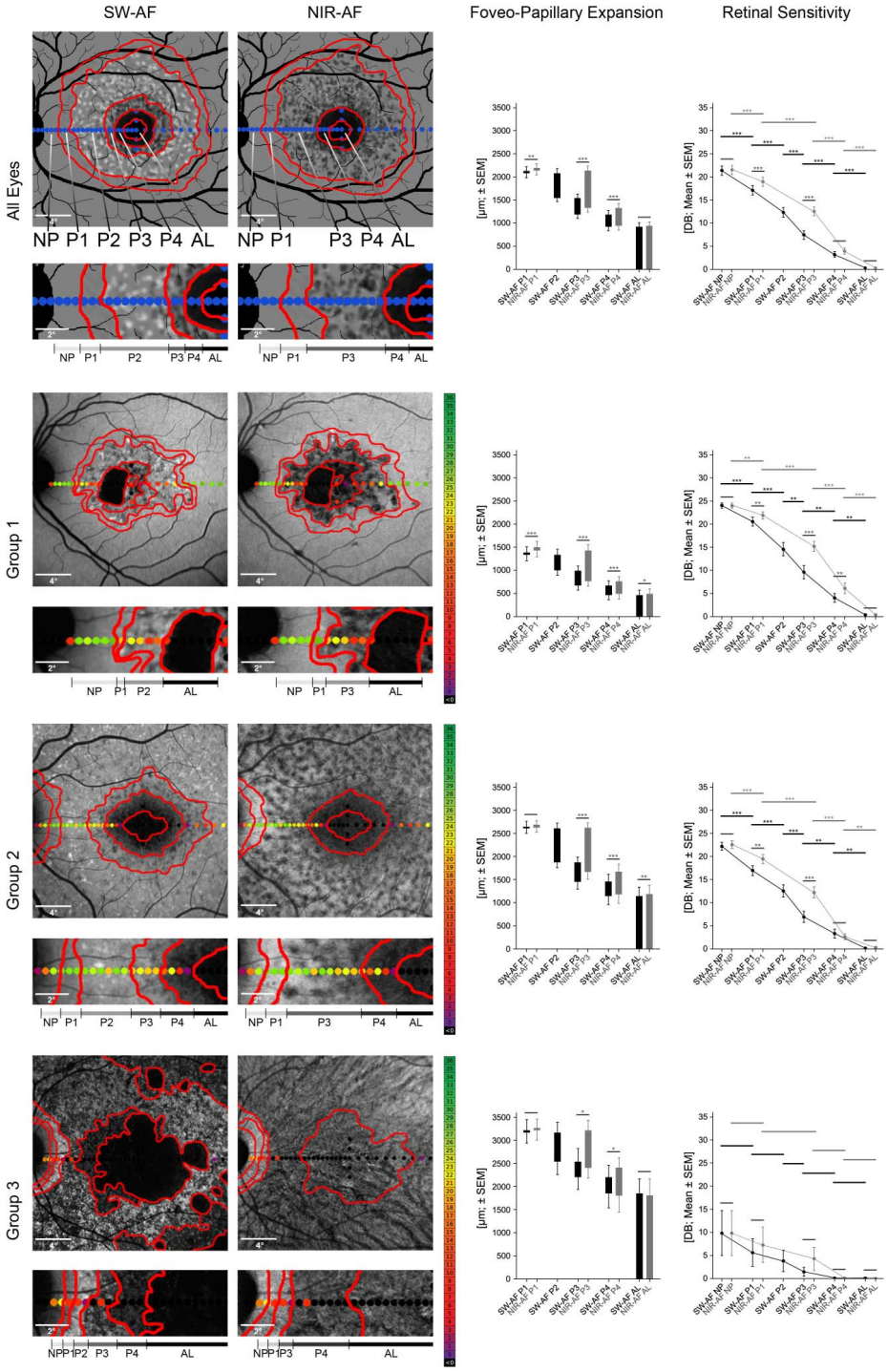

Figure 2. Topography and functional relevance of fundus autofluorescence patterns. SW and NIR-AF images (*left*) as well as foveo-papillary expansion and retinal sensitivity of the different AF patterns (*right*) overall (*top row*) as well as for the different subgroups (*second to last row*). AF patterns were categorized according to their appearance and showed a consistent sequence from the optic nerve head to the fovea (highlighted in *gray dashed frame*): No pattern (NP), granular pattern (P1), flecks of increased (P2) and decreased (P3) AF, irregular dark pattern (P4), atrophic lesions (AL). The foveo-papillary expansion of each AF pattern in NIR-AF, except for AL, exceeded the respective pattern in SW-AF images. Analysis of retinal sensitivity (mean ± SEM) revealed a significant reduction of retinal sensitivity from peripheral to central AF patterns in all eyes and each group, apart from group 3, which showed a general marked reduction, even in NP areas (*$P < 0.05$; **$P < 0.01$; ***$P < 0.001$).

Table 1. Demographic and Genetic Data of Groups Based on Full-Field ERG Results

Group (eyes/patients)[a]	Sex, *n* (%) F	Sex, *n* (%) M	Age, y, Mean ± SEM	Onset, y, Mean ± SEM	p.Gly1961Glu Mutation No. (%)
Group 1 ($n = 42/21$)	16 (76)	5 (24)	32.9 ± 3.2	20.8 ± 2.5	13 (62)
Group 2 ($n = 34/17$)	11 (65)	6 (35)	44.8 ± 4.5	27.7 ± 3.7	2 (12)
Group 3 ($n = 12/6$)	5 (83)	1 (17)	33.8 ± 4.6	18.3 ± 6.2	0 (0)
Total ($n = 88/44$)	32 (73)	12 (27)	37.6 ± 2.5	23.1 ± 21.8	15 (34)
*Group comparisons, *P* value	0.619		0.149	0.203	<0.001

F, female; M, male.
[a] Numbers in columns 2 to 5 refer to patients.
* ANOVA between groups.

subclassified using the full-field ERG-based classification recommended by Lois and colleagues[30]: Group 1 included eyes with normal responses on scotopic and photopic full-field ERG; group 2 included eyes with normal scotopic responses but reduced (over 2 SD) photopic B-wave and 30-Hz flicker amplitudes, and group 3 included eyes with ERG reductions involving both rod- and cone-driven responses.

Statistical Analysis

Statistical analysis was performed with commercially available statistical software (GraphPad Prism 6.0; GraphPad Software, La Jolla, CA) using one factorial analysis of variance (ANOVA) followed by Tukey's test for the pairwise comparison of groups or paired *t*-test after averaging the results of both eyes. Using a 95% significance level, P values < 0.05 were regarded as significant. Correlations between AF alterations and OCT changes were investigated using Spearman's rank correlation coefficient. Interrater reliability between the two readers was assessed with the two-way agreement interclass correlation coefficient (ICC) using the software environment R (version 3.2.3; The R Foundation for Statistical Computing, Vienna, Austria).

Results

Cohort Characteristics

A total of 88 eyes of 44 patients (32 female [73%]) with a mean age at examination of 37.6 ± 2.5 years (±SEM; range, 9–77 years) were included in this study (Table 1, Supplementary Table S1). Forty-one patients were found to have two disease-causing mutations. Three patients had only one disease-causing mutation but showed a phenotype consistent with *ABCA4*-related retinopathy.

Based on the ERG-based classification presented above, 42 eyes were assigned to group 1, 34 eyes to group 2, and 12 eyes to group 3. This classification closely correlated with AF phenotypes, with group 1 encompassing eyes with a localized low signal at the fovea surrounded by single flecks and a homogeneous background, group 2 with a localized low signal at the macula surrounded by a heterogeneous background with numerous foci of abnormal signal (i.e., hyper- and hypoautofluorescent flecks), and group 3 with multiple low signal areas at the posterior pole with a heterogeneous background (Supplementary Fig. S1).[31,32] Both eyes of each patient always met the same group criteria in our study cohort. As demonstrated previously,[33,34] patients assigned to group 1 revealed the common mild p.Gly1961Glu-variant significantly more frequently than did patients assigned to other groups. Distribution of age, age of onset, and sex was not different between subgroups (Table 1).

Fundus AF Patterns

All eyes showed a consistent centrifugal sequence of AF patterns along the foveo-papillary line (foveo-papillary expansion) in both AF modalities overall and throughout the three different groups (Fig. 2, Table 2): Atrophic lesions (AL), an irregular dark pattern (P4), flecks of decreased AF (P3), flecks of increased AF (P2), a granular pattern (P1), and no pattern with a homogeneous background (NP). Due to the rarity of larger areas of P2 on NIR-AF images, individual flecks of increased AF were integrated into P3 (Fig. 2 and Supplementary Fig. S1). In 19 cases (22% representing eyes of each group), the expansion of further single AF patterns (in one or both AF modalities) was not delineable due to absence in the

Table 2. Topography of Fundus AF Alterations

	Foveo-Papillary Expansion, Eccentric Border, Mean ± SEM, μm					
	All Eyes, $n = 88$			Group 1, $n = 42$		
AF Pattern Category	SW-AF	NIR-AF	*P* Value	SW-AF	NIR-AF	*P* Value
No pattern (NP)	—	—	—	—	—	—
Granular pattern (P1)	2119 ± 99	2183 ± 91	0.005	1379 ± 93	1492 ± 90	0.003
Flecks of increased AF (P2)	2073 ± 99	—	—	1326 ± 92	—	—
Flecks of decreased AF (P3)	1541 ± 83	2129 ± 96	<0.001	0990 ± 81	1416 ± 95	<0.001
Irregular dark pattern (P4)	1180 ± 85	1322 ± 90	<0.001	0667 ± 80	0734 ± 80	0.009
Atrophic lesions (AL)	0918 ± 87	0937 ± 89	0.143	0462 ± 78	0486 ± 81	0.008

SEM, standard error of the mean.
* ANOVA between all three groups.

Table 2. Extended

	Foveo-Papillary Expansion, Eccentric Border, Mean ± SEM, μm						
	Group 2, $n = 34$			Group 3, $n = 12$			Group Comparison*
AF Pattern Category	SW-AF	NIR-AF	*P* Value	SW-AF	NIR-AF	*P* Value	*P* Value
No pattern (NP)	—	—	—	—	—	—	—
Granular pattern (P1)	2646 ± 87	2685 ± 69	0.303	3213 ± 180	3258 ± 133	0.657	<0.001
Flecks of increased AF (P2)	2612 ± 85	—	—	3162 ± 181	—	—	<0.001
Flecks of decreased AF (P3)	1871 ± 83	2628 ± 83	<0.001	2536 ± 194	3213 ± 165	0.002	<0.001
Irregular dark pattern (P4)	1455 ± 110	1668 ± 115	<0.001	2198 ± 180	2402 ± 161	0.008	<0.001
Atrophic lesions (AL)	1152 ± 135	1188 ± 136	<0.001	1852 ± 215	1804 ± 258	0.600	<0.001

foveo-papillary area. This did not affect the sequence itself, similar to foveal noninvolvement, which was present in 25 eyes (28%). The consistent sequence simply started paracentrally in the latter (Fig. 2, second row).

Hyperautofluorescent flecks (P2) revealed the largest expansion of AF patterns in SW-AF, whereas hypoautofluorescent flecks (P3) represented the predominant AF pattern in NIR-AF. The eccentricity of NIR-AF patterns significantly exceeded those of SW-AF ($P \leq 0.005$), except for AL ($P = 0.143$; Fig. 2, Table 2). The most obvious difference between both imaging modalities was found for hypoautofluorescent flecks (P3): The area of P3 in NIR-AF images covered most of the area of P2 as well as the area of P3 on SW-AF and even extended more peripherally (Fig. 2, Table 2).

The foveo-papillary expansion of all individual AF patterns increased from group 1 to 3, with the NIR-AF patterns being more eccentric compared to SW-AF patterns (Fig. 2, Table 2). There was a good correlation between both eyes of individual patients (Pearson correlation for NIR-AF and SW-AF measures, $\rho = 0.897$ and $\rho = 0.908$).

Functional Relevance of AF Patterns

Areas with AF alterations in both AF modalities revealed reduced retinal sensitivity, whereas regions with homogenous background (NP) showed relatively preserved retinal function. In accordance with the centrifugal sequence of AF patterns, an increase of retinal sensitivity was found from the central advanced lesions to the more peripheral patterns along the foveo-papillary line (Fig. 2, Table 3). In SW-AF, the main difference in retinal sensitivity was found between regions with hyperfluorescent flecks (P2) and adjacent areas (P1 and P3). In line with the more eccentric AF patterns, NIR-AF patterns showed a generally better mean retinal sensitivity compared to SW-AF, which was significant for areas with a granular pattern (P1) and areas with hypofluorescent flecks (P3; Fig. 2, Table 3). Retinal sensitivity varied most between regions with hypofluorescent flecks (P3) and adjacent areas (P1 and P4) in this AF modality.

In the subgroup analysis, group 1 and 2 eyes showed overall comparable retinal sensitivity throughout the different AF patterns with only slightly lower retinal sensitivity in group 2. In contrast, group 3 eyes

Table 3. Retinal Sensitivity of Fundus AF Alterations

	Retinal Sensitivity, Mean ± SEM, dB					
	All Patients, $n = 88$			Group 1, $n = 42$		
AF Pattern Category	SW-AF	NIR-AF	*P* Value	SW-AF	NIR-AF	*P* Value
No pattern (NP)	21.41 ± 0.75	21.54 ± 0.75	0.053	24.06 ± 0.44	24.06 ± 0.45	0.986
Granular pattern (P1)	17.13 ± 0.80	18.97 ± 0.77	<0.001	20.56 ± 0.79	21.93 ± 0.70	0.011
Flecks of increased AF (P2)	12.33 ± 0.78	—	—	14.58 ± 1.05	—	—
Flecks of decreased AF (P3)	07.48 ± 0.73	12.56 ± 0.71	<0.001	9.64 ± 1.10	15.20 ± 0.89	<0.001
Irregular dark pattern (P4)	03.15 ± 0.53	03.97 ± 0.55	0.080	3.98 ± 0.84	06.15 ± 0.95	<0.001
Atrophic lesions (AL)	00.29 ± 0.10	00.32 ± 0.11	0.258	0.45 ± 0.20	00.47 ± 0.22	0.661

* ANOVA between all three groups.

Table 3. Extended

	Retinal Sensitivity, Mean ± SEM, dB						
	Group 2, $n = 34$			Group 3, $n = 12$			Group Comparisons*
AF Pattern Category	SW-AF	NIR-AF	*P* Value	SW-AF	NIR-AF	*P* Value	*P* Value
No pattern (NP)	22.20 ± 0.65	22.55 ± 0.64	0.026	09.83 ± 3.46	09.83 ± 3.46	1.000	<0.001
Granular pattern (P1)	16.96 ± 0.98	19.44 ± 0.81	0.006	05.60 ± 0.20	7.27 ± 2.72	0.103	<0.001
Flecks of increased AF (P2)	12.55 ± 1.07	—	—	3.84 ± 1.66	—	—	<0.001
Flecks of decreased AF (P3)	6.93 ± 1.04	12.22 ± 0.93	<0.001	1.46 ± 0.97	04.25 ± 1.74	0.077	<0.001
Irregular dark pattern (P4)	3.23 ± 0.84	02.65 ± 0.55	0.514	0.08 ± 0.08	00.10 ± 0.07	0.445	<0.001
Atrophic lesions (AL)	0.18 ± 0.09	00.24 ± 0.11	0.058	0.06 ± 0.06	00.00 ± 0.00	0.339	0.113

revealed a more severe functional impairment associated with each AF pattern, resulting in a lower mean difference between the different AF patterns. The only exception was found in areas with AL where retinal function was poor throughout all groups (Fig. 2).

Structural Correlates of AF Pattern

On OCT imaging, patients with *ABCA4*-related retinopathy showed characteristic alterations of the outer retina (Fig. 3). A characteristic sequence was found along the foveo-papillary line, with loss of the EZ being most and RPE loss being least widespread, that revealed a good correlation between both eyes of individual patients (Pearson correlation, $\rho = 0.889$). Comparisons with AF patterns revealed a correlation of total hypoautofluorescent pattern (i.e., P3, P4, and AL) in NIR-AF and the hypo- and hyperautofluorescent alterations (i.e., P2, P3, P4, and AL) in SW-AF with the EZ loss ($r = 0.971$; $P < 0.001$ and $r = 0.979$, $P < 0.001$). The expansion of hypoautofluorescent pattern (i.e., P3, P4, and AL) in SW-AF correlated with the extension of the ELM loss ($r = 0.933$, $P < 0.001$). Within the area of AL, OCT revealed a disrupted RPE band and associated hyperreflectivity of the underlying tissues (i.e., choroid). However, OCT hyperreflectivity was not consistently restricted to AL and was often discontinuous. Regarding the most eccentric granular pattern (P1), no corresponding OCT alteration was found. Therefore, the total foveo-papillary expansion of alterations in both AF modalities significantly exceeded those of OCT lesions ($P < 0.001$).

Interrater Agreement

The measurements of foveo-papillary expansion exhibited an excellent interrater agreement of 0.936 (ICC; 95% confidence interval [CI]: 0.928, 0.943) for overall measurements, 0.927 (0.913, 0.939) for SW-AF, 0.928 (0.914, 0.940) for NIR-AF, and 0.989 (0.982, 0.992) for OCT grading.

Discussion

In this study, we evaluated the association of different AF patterns with retinal function and OCT alterations in *ABCA4*-related retinopathy. In accordance with the centrifugal expansion of the disease,[15,25] a consistent sequence of different AF patterns ranging from AL to homogeneous back-

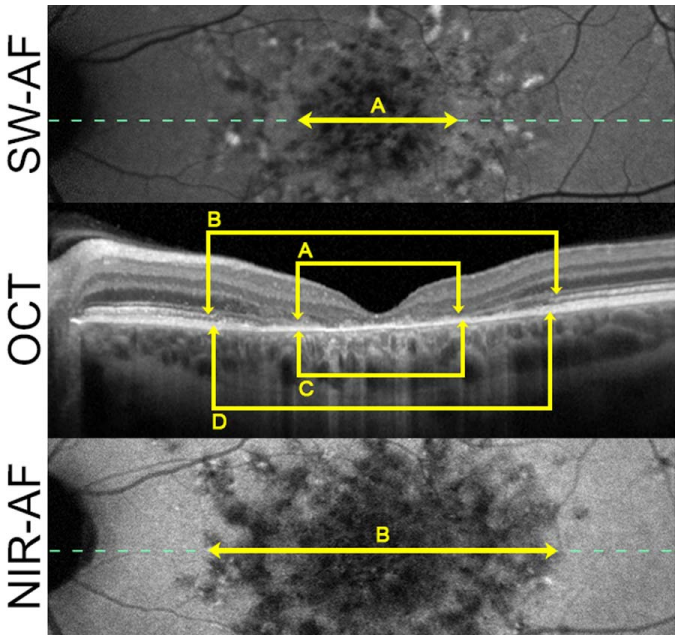

Figure 3. Structural correlates of AF patterns. Composite picture of SW-AF (*top*), OCT (*middle*), and NIR-AF (*bottom*) images of a characteristic patient with *ABCA4*-related retinopathy illustrates the correlation between imaging modalities. The pattern of flecks with decreased AF (P3) in NIR-AF images (B) and SW-AF images (A) were associated with loss of the EZ band (C) and loss of the ELM (D), respectively. The *dotted line* marks the location of the horizontal OCT scan.

ground (NP) was identified that correlated with gradual normalization of functional impairment (i.e., from loss of light sensitivity in AL to mild impairment in P1 and preserved function in NP; Fig. 2) and OCT alterations (i.e., from loss of multiple OCT layers in AL to regular OCT appearance in P1 and NP), indicating different disease stages.

In accordance with previous reports,[13,15–20,22] the individual NIR-AF patterns exceeded those on SW-AF, suggesting that changes on NIR-AF preceed those on SW-AF (Fig. 2, Table 2). Similar findings have been described for retinitis pigmentosa or choroideremia, suggesting that NIR-AF might have the general potential to detect damage/dysfunction of the RPE earlier.[35–37] The most widespread AF patterns were hypofluorescent flecks (P3) in NIR-AF and hyperfluorescent flecks (P2) in SW-AF, respectively. The peripheral borders of these patterns correlated with EZ loss and showed the most distinct change of retinal sensitivity in comparison to adjacent regions (Figs. 2 and 3), suggesting that the occurrence of these patterns might represent an important stage of retinal degeneration in *ABCA4*-related retinopathy. Subgroup analysis based on a full-field ERG classification revealed generally comparable results, validating these findings for different disease manifestations and stages of *ABCA4*-related retinopathy. However, in accordance with the increasing dysfunction of rods and cones from group 1 to 3, eyes assigned to group 2 and especially group 3 showed an increasing expansion of AF alterations and severity of functional impairment (Fig. 2) underlining previous reports.[31,38] As the distinct functional impairment in group 3 eyes was present throughout the AF patterns along the foveo-papillary line (including the most eccentric pattern), the loss of retinal sensitivity quickly reached the end of the dynamic range of the microperimetry device (indicated by 0 dB). Therefore, the visualized slope of the functional decline in Figure 2 seemed shallower compared to group 1 and 2 eyes (irrespective of artificial *x*-axis dimensions).

Pathophysiological Considerations

Based on our results, it can be hypothesized that the described AF patterns represent different stages of disease progression as suggested in a previous report of a small study cohort ($n = 7$ patients) with *ABCA4*-related retinopathy:[14] (1) We found a sequence of observed AF pattern from the fovea to the optic nerve head. This particular sequence was shown to be consistent throughout our cohort irrespective of phenotypic presentation, general retinal involvement, or foveal status. (2) The retinal sensitivity differed between the areas of these different AF patterns and declined in association with the AF sequence, implying the functional relevance of the AF findings. (3) We found structural correlates in OCT images, with more pronounced changes demarcating more severe AF patterns.

Early- to late-stage AF changes in both AF modalities can be explained by the disease characteristic pathophysiology. An early finding in *ABCA4*-related retinopathy is an accumulation of lipofuscin granules within the RPE that is reflected by generally increased AF signal as measured, for example, by quantitative fundus AF imaging. Of note, this accumulation is not associated with a pattern on AF images, and retinal structure assessed by OCT appears relatively preserved. Accordingly, these areas presented relatively preserved retinal function (especially in group 1 and 2 eyes; Fig. 2, Table 3),[39] suggesting that lipofuscin accumulation itself is not associated with clinically relevant functional impairment.

Next, there is occurrence of hyperautofluorescent flecks on SW and NIR-AF. The histopathologic

correlate of hyperautofluorescent flecks on SW-AF might be accumulation of lipofuscin granules within the RPE.[40,41] The explanation of hyperautofluorescent flecks on NIR-AF is less intuitive but may include apical displacement of intracellular melanin granules by lipofuscin or formation of derivates such as melano-lipofuscin and oxidized melanin. Further accumulation of lipofuscin granules is then suggested to lead to loss of melanin granules. This may be an explanation for the widespread occurrence of hypoautofluorescent flecks on NIR-AF within the area of hyperautofluorescent flecks on SW-AF.[17] An alternative hypothesis states that fluorophores at photoreceptor level can also account for the increased SW-AF signal and that the reduced AF signal on NIR-AF might already represent early RPE atrophy.[16,17,22] This would be an important hint that RPE degeneration might precede photoreceptor degeneration. In addition, there is evidence for heterogeneity and a possible remodeling of fluorophore components during disease progression. This is indicated, for example, by spectrally resolved AF imaging showing longer wavelength emission in eccentric flecks compared to shorter wavelength emission in central flecks,[42] as well as distinct differences between central and eccentric flecks in fluorescence lifetime imaging ophthalmoscopy.[43]

As a final stage, RPE undergoes cell death, also visible on OCT imaging, leading to irregular dark pattern (P4) and AL in both AF modalities.[35] Hypoautofluorescent flecks (P3) in SW-AF seem to be an interstate with a delicate structural alteration affecting photoreceptor integrity associated with ELM loss or thinned retinal layers.[18,44] Therefore, further evaluation of differences between hyperautofluorescent flecked (P2) and hypoautofluorescent flecked (P3) pattern in SW-AF may provide more insights into disease pathomechanisms.

Explanations for the more severe functional impairment in group 3 eyes compared to eyes assigned to both other groups despite similar AF alterations (i.e., different retinal sensitivity in the same AF pattern) can only be hypothesized. For example, a compromised choroid (as found in group 3)[34] could impair the exchange of hitherto unknown neuroprotective factors and nutrients that might lead to an increased accumulation of toxic compounds and activation of inflammatory processes resulting in accelerated functional decline in group 3. This might be an interesting target for further molecular research.

Relevance for Assessment of Progression and Treatment Effects

The definition of clinical endpoints is essential for reliably recording disease progression and potential treatment effects. As patients with *ABCA4*-related retinopathy typically reveal either early loss of visual acuity due to early foveal involvement or long-term preservation of visual acuity in the case of foveal noninvolvement, BCVA does not represent a suitable outcome parameter. Novel high-resolution imaging modalities such as AF provide objective in vivo measures of disease alterations in a time- and resource-effective manner.[45] However, the often-proposed assessment of RPE atrophy might not be an ideal clinical endpoint in *ABCA4*-related retinopathy as this disease stage might already represent a point of no return at which treatment effects are more difficult to achieve.[23] In addition, progression rates of RPE atrophy secondary to *ABCA4*-related retinopathy are distinctly slower compared to other retinal degenerations such as AMD,[46] making the detection of potential treatment effects challenging. As AL are surrounded by distinguishable zones of characteristic AF patterns, these patterns might be an interesting alternative as outcome parameters for future treatment trials. As outlined above, these zones might represent different stages of degeneration that may show different responses to treatments and hence could be more useful for the detection of individual treatment effects. However, the potential of these AF alterations as clinical endpoints needs to be investigated in more detail in the future, for example, in longitudinal studies.

From a more general perspective, the use of NIR-AF might have several advantages over SW-AF in clinical routines as well as clinical studies as follows. (1) NIR-AF imaging might be an earlier marker of disease-associated alterations and progression. (2) The less-energetic long-wavelength light reduces the potential risk of toxic effects.[47,48] (3) There is no masking by macular pigment leading to an improved assessment of the foveal region.[31] (4) The long-wavelength excitation light causes less impairment by optic media opacities (i.e., cataract)[49] and (5) significantly less glare. In this study, each of our subjects described discomfort and difficulty in keeping the fixation due to glare during the SW-AF imaging, while NIR-AF was not associated with similar effects (anecdotal evidence). This indicates a potential superiority over SW-AF in the management of *ABCA4*-related retinopathy. However, the long-term experience with SW-AF and the possibility of studying different

pathophysiological pathways favors the use of both AF modalities, at least in an experimental setup.

In conclusion, this study revealed a sequence of AF patterns in *ABCA4*-related retinopathy that correlated with functional impairment and structural alterations on OCT imaging (Figs. 2 and 3). These findings might help to broaden the pathophysiological understanding of *ABCA4*-related retinopathy and might be of particular value for future treatment studies. Alterations of NIR-AF appear to precede those of SW-AF, suggesting superiority in detecting early disease progression as well as the theoretically reduced risk of phototoxicity and the better visualization of the central macula.

Acknowledgments

This work was supported by the ProRetina Deutschland, Aachen, Germany; the Association of Rhine-Westphalian Ophthalmologists, Recklinghausen, Germany; the German Ophthalmological Society and the German Research Foundation (Grants MU4279/1-1, MU4279/2-1, and GL920/1-1), and the National Institute for Health Research Oxford Biomedical Research Centre. The funding organizations had no role in the design and conduct of the study; collection, management, analysis, and interpretation of the data; preparation, review, or approval of the manuscript; and decision to submit the manuscript for publication.

Disclosure: **P.L. Müller**, Heidelberg Engineering (F), Optos (F), Carl Zeiss MedicTec (F), CenterVue (F); **J. Birtel**, Heidelberg Engineering (F), Optos (F), Carl Zeiss MedicTec (F), CenterVue (F); **P. Herrmann**, Heidelberg Engineering (F), Optos (F), Carl Zeiss MedicTec (F), CenterVue (F); **F.G. Holz**, Heidelberg Engineering (F, C, R), Optos (F), Carl Zeiss MedicTec (F, C), CenterVue (F), Allergan (F, R), Alcon/Novartis (F, R), Genentech/Roche (F, R), Bayer (F, R), Acucela (F, R), Boehringer Ingelheim (F, R), LinBioscience (F), Grayburg (F), Nightstar (F); **P. Charbel Issa**, None; **M. Gliem**, Heidelberg Engineering (F), Optos (F), Carl Zeiss MedicTec (F), CenterVue (F)

References

1. Hamel CP. Cone rod dystrophies. *Orphanet J Rare Dis*. 2007;2:1–7.
2. Kitiratschky VBD, Grau T, Bernd A, et al. ABCA4 gene analysis in patients with autosomal recessive cone and cone rod dystrophies. *Eur J Hum Genet*. 2008;16:812–819.
3. Birtel J, Eisenberger T, Gliem M, et al. Clinical and genetic characteristics of 251 consecutive patients with macular and cone/cone-rod dystrophy. *Sci Rep*. 2018;8:4824.
4. Allikmets R, Singh N, Sun H, et al. A photoreceptor cell-specific ATP-binding transporter gene (ABCR) is mutated in recessive Stargardt macular dystrophy. *Nat Genet*. 1997;15:236–246.
5. Koenekoop RK. The gene for Stargardt disease, ABCA4, is a major retinal gene: a mini-review. *Ophthalmic Genet*. 2003;24:75–80.
6. Mata NL, Weng J, Travis GH. Biosynthesis of a major lipofuscin fluorophore in mice and humans with ABCR-mediated retinal and macular degeneration. *Proc Natl Acad Sci U S A*. 2000;97:7154–7159.
7. Sears AE, Bernstein PS, Cideciyan AV, et al. Towards treatment of Stargardt disease: workshop organized and sponsored by the Foundation Fighting Blindness. *Transl Vis Sci Technol*. 2017;6:6.
8. Müller PL, Gliem M, Mangold E, et al. Monoallelic ABCA4 mutations appear insufficient to cause retinopathy: a quantitative autofluorescence study. *Invest Ophthalmol Vis Sci*. 2015;56:8179–8186.
9. Burke TR, Duncker T, Woods RL, et al. Quantitative fundus autofluorescence in recessive Stargardt disease. *Invest Ophthalmol Vis Sci*. 2014;55:2841–2852.
10. Delori FC, Dorey CK, Staurenghi G, Arend O, Goger DG, Weiter JJ. In vivo fluorescence of the ocular fundus exhibits retinal pigment epithelium lipofuscin characteristics. *Invest Ophthalmol Vis Sci*. 1995;36:718–729.
11. Delori FC, Staurenghi G, Arend O, Dorey CK, Goger DG, Weiter JJ. In vivo measurement of lipofuscin in Stargardt's disease–fundus flavimaculatus. *Invest Ophthalmol Vis Sci*. 1995;36:2327–2331.
12. Cideciyan AV, Aleman TS, Swider M, et al. Mutations in ABCA4 result in accumulation of lipofuscin before slowing of the retinoid cycle: a reappraisal of the human disease sequence. *Hum Mol Genet*. 2004;13:525–534.
13. Keilhauer CN, Delori FC. Near-infrared autofluorescence imaging of the fundus: visualization of ocular melanin. *Invest Ophthalmol Vis Sci*. 2006;47:3556–3564.

14. Cideciyan AV, Swider M, Aleman TS, et al. Reduced-illuminance autofluorescence imaging in ABCA4-associated retinal degenerations. *J Opt Soc Am A*. 2007;24:1457.
15. Cukras C, Wong W, Caruso R, Cunningham D, Zein W, Sieving P. Centrifugal expansion of fundus autofluorescence patterns in Stargardt disease over time. *Arch Ophthalmol*. 2012;130: 171–179.
16. Sparrow JR, Marsiglia M, Allikmets R, et al. Flecks in recessive Stargardt disease: short-wavelength autofluorescence, near-infrared autofluorescence, and optical coherence tomography. *Invest Ophthalmol Vis Sci*. 2015;56:5029–5039.
17. Duncker T, Marsiglia M, Lee W, et al. Correlations among near-infrared and short-wavelength autofluorescence and spectral-domain optical coherence tomography in recessive Stargardt disease. *Invest Ophthalmol Vis Sci*. 2014;55: 8134–8143.
18. Greenstein VC, Schuman AD, Lee W, et al. Near-infrared autofluorescence: its relationship to short-wavelength autofluorescence and optical coherence tomography in recessive Stargardt disease. *Invest Ophthalmol Vis Sci*. 2015;56: 3226–3234.
19. Kellner S, Kellner U, Weber BHF, Fiebig B, Weinitz S, Ruether K. Lipofuscin- and melanin-related fundus autofluorescence in patients with ABCA4-associated retinal dystrophies. *Am J Ophthalmol*. 2009;147:895–902, 902.e1.
20. Cideciyan AV, Swider M, Schwartz SB, Stone EM, Jacobson SG. Predicting progression of ABCA4-associated retinal degenerations based on longitudinal measurements of the leading disease front. *Invest Ophthalmol Vis Sci*. 2015; 56:5946–5955.
21. Greenstein VC, Nunez J, Lee W, et al. A comparison of en face optical coherence tomography and fundus autofluorescence in Stargardt disease. *Invest Ophthalmol Vis Sci*. 2017;58:5227–5236.
22. Paavo M, Lee W, Allikmets R, Tsang S, Sparrow JR. Photoreceptor cells as a source of fundus autofluorescence in recessive Stargardt disease. *J Neurosci Res*. 2019;97:98–106.
23. Cideciyan AV, Swider M, Aleman TS, et al. Macular function in macular degenerations: repeatability of microperimetry as a potential outcome measure for ABCA4-associated retinopathy trials. *Invest Ophthalmol Vis Sci*. 2012;53: 841–852.
24. Parodi MB, Iacono P, Triolo G, et al. Morpho-functional correlation of fundus autofluorescence in Stargardt disease. *Br J Ophthalmol*. 2015;99: 1354–1359.
25. Strauss RW, Muñoz B, Ho A, et al. Progression of Stargardt disease as determined by fundus autofluorescence in the Retrospective Progression of Stargardt Disease Study (ProgStar Report No. 9). *JAMA Ophthalmol*. 2017;135:1232–1241.
26. Sergouniotis PI, McKibbin M, Robson AG, et al. Disease expression in autosomal recessive retinal dystrophy associated with mutations in the DRAM2 gene. *Invest Ophthalmol Vis Sci*. 2015; 56:8083–8090.
27. Johnson CA, Chauhan BC, Shapiro LR. Properties of staircase procedures for estimating thresholds in automated perimetry. *Invest Ophthalmol Vis Sci*. 1992;33:2966–2974.
28. Troeger E, Sliesoraityte I, Charbel Issa P, Scholl HN, Zrenner E, Wilke R. An integrated software solution for multi-modal mapping of morphological and functional ocular data. In: *2010 Annual International Conference of the IEEE Engineering in Medicine and Biology*. Vol. 2010. New York, NY: IEEE; 2010:6280–6283.
29. Kuehlewein L, Hariri AH, Ho A, et al. Comparison of manual and semiautomated fundus autofluorescence analysis of macular atrophy in Stargardt disease phenotype. *Retina*. 2016;36: 1216–1221.
30. Lois N, Holder GE, Bunce C, Fitzke FW, Bird AC. Phenotypic subtypes of Stargardt macular dystrophy-fundus flavimaculatus. *Arch Ophthalmol*. 2001;119:359–369.
31. Müller PL, Pfau M, Mauschitz MM, et al. Comparison of green versus blue fundus autofluorescence in ABCA4-related retinopathy. *Transl Vis Sci Technol*. 2018;7:13.
32. Fujinami K, Lois N, Mukherjee R, et al. A longitudinal study of Stargardt disease: quantitative assessment of fundus autofluorescence, progression, and genotype correlations. *Invest Ophthalmol Vis Sci*. 2013;54:8181–8190.
33. Cella W, Greenstein VC, Zernant-Rajang J, et al. G1961E mutant allele in the Stargardt disease gene ABCA4 causes bull's eye maculopathy. *Exp Eye Res*. 2009;89:16–24.
34. Müller PL, Fimmers R, Gliem M, Holz FG, Charbel Issa P. Choroidal alterations in ABCA4-related retinopathy. *Retina*. 2017;37:359–367.
35. Cideciyan AV, Swider M, Jacobson SG. Autofluorescence imaging with near-infrared excitation: normalization by reflectance to reduce signal from choroidal fluorophores. *Invest Opthalmol Vis Sci*. 2015;56:3393.

36. Duncker T, Tabacaru MR, Lee W, Tsang SH, Sparrow JR, Greenstein VC. Comparison of near-infrared and short-wavelength autofluorescence in retinitis pigmentosa. *Invest Ophthalmol Vis Sci*. 2013;54:585–591.
37. Birtel J, Salvetti AP, Jolly JK, et al. Near-infrared autofluorescence in choroideremia: anatomic and functional correlations. *Am J Ophthalmol*. 2019; 199:19–27.
38. Lois N, Halfyard AS, Bird AC, Holder GE, Fitzke FW. Fundus autofluorescence in Stargardt macular dystrophy-fundus flavimaculatus. *Am J Ophthalmol*. 2004;138:55–63.
39. Pfau M, Lindner M, Fleckenstein M, et al. Test-retest reliability of scotopic and mesopic fundus-controlled perimetry using a modified MAIA (Macular Integrity Assessment) in normal eyes. *Ophthalmologica*. 2017;237:42–54.
40. Eagle RC, Lucier AC, Bernardino VB, Yanoff M. Retinal pigment epithelial abnormalities in fundus flavimaculatus: a light and electron microscopic study. *Ophthalmology*. 1980;87:1189–1200.
41. Lopez PF, Maumenee IH, de la Cruz Z, Green WR. Autosomal-dominant fundus flavimaculatus. Clinicopathologic correlation. *Ophthalmology*. 1990;97:798–809.
42. Dysli C, Müller PL, Birtel J, Holz FG, Herrmann P. Spectrally resolved fundus autofluorescence in ABCA4-related retinopathy. *Invest Ophthalmol Vis Sci*. 2019;60:274–281.
43. Dysli C, Wolf S, Hatz K, Zinkernagel MS. Fluorescence lifetime imaging in Stargardt disease: potential marker for disease progression. *Invest Ophthalmol Vis Sci*. 2016;57:832–841.
44. Lee W, Nõupuu K, Oll M, et al. The external limiting membrane in early-onset Stargardt disease. *Invest Ophthalmol Vis Sci*. 2014;55:6139–6149.
45. Birtel J, Gliem M, Holz FG, Herrmann P. [Imaging and molecular genetic diagnostics for the characterization of retinal dystrophies]. *Ophthalmologe*. 2018;115:1021–1027.
46. McBain VA, Townend J, Lois N. Progression of retinal pigment epithelial atrophy in stargardt disease. *Am J Ophthalmol*. 2012;154:146–154.
47. Sparrow JR, Nakanishi K, Parish CA. The lipofuscin fluorophore A2E mediates blue light-induced damage to retinal pigmented epithelial cells. *Invest Ophthalmol Vis Sci*. 2000;41:1981–1989.
48. Dorey CK, Delori FC, Akeo K. Growth of cultured RPE and endothelial cells is inhibited by blue light but not green or red light. *Curr Eye Res*. 1990;9:549–559.
49. Boettner EA, Wolter JR. Transmission of the ocular media. *Invest Ophthalmol Vis Sci*. 1962;1: 776–783.